University of Groningen

Periodic Hartree-Fock and hybrid density functional calculations on the metallic and the insulating phase of (EDO-TTF)(2)PF6

Linker, Gerrit-Jan; van Loosdrecht , Paul H. M.; van Duijnen , Piet Th.; Broer, Ria

Link to publication in University of Groningen/UMCG research database

CrossMark
click for updates

Periodic Hartree–Fock and hybrid density functional calculations on the metallic and the insulating phase of (EDO-TTF)₂PF₆†

Gerrit-Jan Linker,*[a] Paul H. M. van Loosdrecht,[b] Piet Th. van Duijnen[a] and Ria Broer[a]

The insulating and conducting phases of (EDO-TTF)$_2$PF$_6$ were studied by all electron, periodic Hartree–Fock and hybrid density functional calculations. Electronic properties, such as the electronic band structure, the density of states and the Fermi surface are discussed in relation to the metal–insulator transition in this material. The nature of conduction is confirmed in both phases from their band structures and density of states. The hybrid DFT band gaps are in good agreement with experiment. Interactions are discussed on the basis of band dispersion in the inter-stack, intra-stack and inter-sheet directions. We discuss the phase transition in terms of the Peierls mechanism and our results fully support this view.

Introduction

The redox salt (EDO-TTF)$_2$PF$_6$ is a synthetic metal that becomes an insulator when cooled below room temperature. This metal–insulator (MI) transition is thought to be the result of several phenomena arising from instabilities in the system: dimerisation, charge ordering (CO) with an associated geometrical ordering and molecular flexibility. There is ample experimental evidence on these instabilities[1–4] however, as of yet the mechanism of the MI transition remains unclear.

In the molecular crystal, the near planar ethylenedioxy-tetrathiafulvalene (EDO-TTF) molecules, see Fig. 1, act as electron donors and stack to form columns. Viewed as being built from these one-dimensional columns, adjacent columns in the material form two-dimensional sheets where the electron accepting PF$_6$ molecules reside in cavities between two columns.
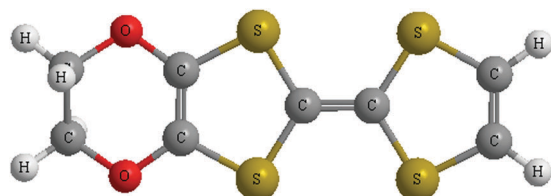

Fig. 1 Top view of the ball-stick representation of EDO-TTF.

[a] *Theoretical Chemistry, Zernike Institute for Advanced Materials, University of Groningen, The Netherlands. E-mail: g.j.linker@rug.nl*
[b] *Physics Institute 2, University of Cologne, Germany*

† Electronic supplementary information (ESI) available: Technical details and technical discussions of the results. See DOI: 10.1039/c5cp05187h

These sheets stack to form the three-dimensional crystal. In Fig. 2 this representation is given for the high temperature (HT) crystal in which all molecules are equivalent. At HT each EDO-TTF molecule donates on average half an electron to a PF$_6$ acceptor molecule. In the crystal at low temperature (LT) adjacent EDO-TTF molecules dimerise. At LT one molecule is neutral with a bent (B) geometry whereas the second molecule bears the positive charge and is planar (P). Earlier, various studies confirmed the strong relation of molecular geometry and charge[2,5,6] and we explained the bent geometry using a classical electromechanical model.[7] For the description of the crystal, a unit cell containing a stack of four EDO-TTF molecules can be taken, see Fig. 2a and b. In terms of such a tetramer unit cell, at LT the crystal exhibits a geometrical ordering (BPPB) that is connected to a charge ordering (0110), both of which are absent in the HT crystal.

The (EDO-TTF)$_2$PF$_6$ molecular crystal is a member of a class of iso-structural organic molecular crystals[8–10] based on a tetra-methyl derivative of TTF and its selenium substituted counterpart TSF: tetramethyl-tetraselenafulvalene (TMTSF) and tetramethyl-tetrathiafulvalene (TMTTF). The salts, referred to as Bechgaard and Fabre salts respectively, are one-dimensional conductors. They were extensively studied in the past after Bechgaard and Jérome[11] discovered the superconducting state in TMTSF with a transition temperature of about 1 K: the first organic super-conductor. In the search for superconductivity at higher temperatures, related materials were synthesised in which many different phases were found:[12] (TMTTF)$_2$X and (TMTSF)$_2$Y with X ∈ {SbF$_6$, AsF$_6$, PF$_6$, Br} and Y ∈ {PF$_6$, ClO$_4$}. Some of these materials have different stacking patterns or exhibit two or three dimensional conductivity. Among the phases found in
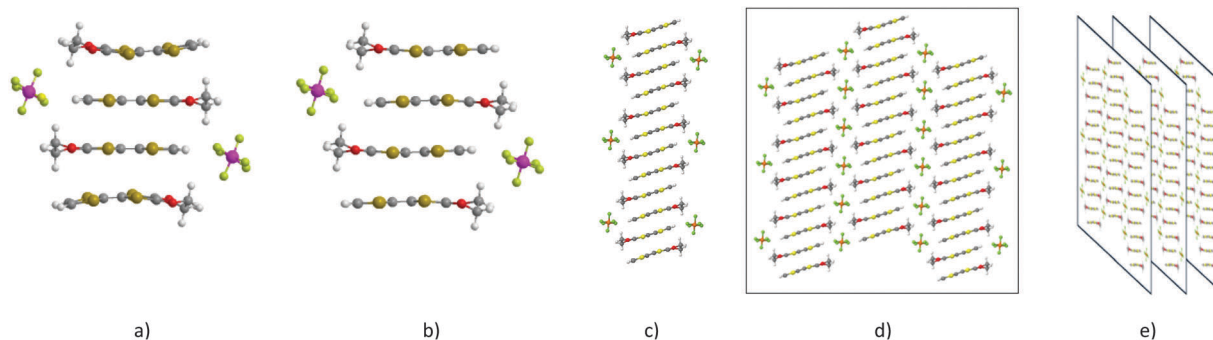
Fig. 2 Visualisation of a tetramer unit cell of the LT (a) and HT (b) crystal. Representation of the HT crystal: a 1D column (c) a 2D sheet of columns (d) and a stack of sheets, the 3D crystal (e).

these materials are: superconductivity, spin-density wave, antiferromagnetism, spin-polarisation, charge-ordering, 1D, 2D and 3D conduction.[13] The material studied in this paper, $(EDO-TTF)_2PF_6$, is not known to display such a complex phase pattern. It shows a first order[14] metal to charge ordered insulator transition just above room temperature (278 K[1]) in strong contrast to $(TMTSF)_2PF_6$ which remains metallic down to a few Kelvin. The charge ordering is thought to result from a Peierls type of electron–phonon interaction in conjunction to anion (PF_6) ordering (AO).[14]

It is reasonable to expect that many of the electronic properties of $(EDO-TTF)_2PF_6$ are determined by the π-electrons at the Fermi level. Therefore, the determination of the π-electron bands and of the Fermi surface is essential to clarify their origin. The small overlap of the π-orbitals of adjacent EDO-TTF molecules in the stack confines the conduction to a narrow conduction channel. The flexibility of the EDO-TTF molecules[6] causes softness of the lattice which, in turn, causes electrons to couple strongly to lattice vibrations.[15] This makes the properties of the material susceptible to external stimuli such as temperature, pressure[16] and light.[17] One of the most intriguing properties of $(EDO-TTF)_2PF_6$ is the ultra-fast and highly efficient photo induced phase transition from the insulating to a metallic state.[17]

Our aim here is to understand the connection between the differences in physical properties of the LT and the HT phase and the differences in the electronic structure. Analysis of the band dispersion can provide confirmation of the Q1D nature and can provide insight into the intermolecular interactions in the crystal. We first analyse the band dispersion in the X-ray crystal structures. Next, we analyse the band dispersion along the three main vectors of translational symmetry. Intermolecular interactions are studied by making scans in the three main molecular directions in the crystals. Therewith we provide a basis for future work to elucidate the mechanisms behind the MI transition. To this end we present the results of all electron periodic calculations. We used Hartree–Fock (HF) theory as well as hybrid density functional theory (DFT) in which some electron correlation is taken into account. The density functionals B3LYP and PBE0 were used. We used spin-restricted theory which we found to be the best ansatz for the ground state in previous work.[18]

Computational details

Periodic, spin-restricted *ab initio* calculations were performed in which the single particle periodic wave functions are built from Bloch functions that are defined in terms of atomic basis functions. RHF calculations were used to connect the crystal calculations to the cluster calculations on the unit cell. Hybrid DFT was employed to account for some electron correlation. We chose B3LYP, which contains 20% Fock exchange, because of our favourable experience with its description of single EDO-TTF molecules.[6] Calculated band gaps are expected to be influenced by the percentage of Fock exchange used. We therefore chose to also perform calculations with the PBE0 hybrid functional,[19] which contains 25% Fock exchange.

In the calculations we used the X-ray structure of Ota, *et al.*[14] Hydrogen positions were obtained from single molecule cluster RHF calculations. The centrosymmetric lattices are triclinic and have the $P\bar{1}$ space group. The structure of the insulating and the metallic phases was determined at 260 K and at 293 K respectively. The LT unit cell contains four EDO-TTF molecules whereas the high temperature unit cell contains two (HT2). The lattice parameters for these crystal structures are (a, b, c, α, β, γ) for LT: 9.822 Å, 11.000 Å, 11.487 Å, 101.865°, 99.128°, 90.445° and for HT: 7.197 Å, 7.343 Å, 11.948 Å, 93.454°, 75.158°, 97.405°. For easier comparison with the tetramer LT crystal, the HT unit cell was doubled in the 1D-columnar direction to make the HT unit cell also contain four EDO-TTF molecules. We refer to the doubled unit cells as HT or HT4.

The basis set used is 6-21G. Linear dependencies are experienced when using basis sets with more diffuse functions, such as 6-31G. Mulliken charge analysis in a molecule in the crystalline environment gives results similar to earlier calculations on the isolated monomer with larger basis sets:[6] the positive charges in $EDO-TTF^+$ molecules are located predominantly on the sulphur atoms. Also a geometry optimisation of the unit cell contents, in which the lattice parameters remain static, shows that the bent and planar molecular geometries are reproduced. In earlier work, we established that the polarisability of the sulphur atoms must be adequately described in order to reproduce the molecular geometry.[7] We conclude that the 6-21G basis set gives a well enough representation of the system.

The CRYSTAL09 computer code[20] was used. The level of accuracy in evaluating the Coulomb and Hartree–Fock exchange series is controlled by five parameters in CRYSTAL: ITOL1-5[21] for which the values 9, 9, 9, 9 and 18 are used. Pack–Monkhorst and Gilat net grids were used with a shrinking factor of 8 to sample k-space. Fermi surfaces and Bloch orbitals were created using DL Visualise.[22]

The HF cluster calculations on a single HT4 unit cell were performed using the MOLCAS code,[23] using the 6-31G** basis set.

Cluster results for one unit cell in vacuum

We use the electronic structure of a HT unit cell cluster in isolation as a reference for discussing the properties of the crystal. First, we consider the neutral tetramer: $(EDO-TTF)_4$. The highest four occupied HF orbitals of the ground state are simply linear combinations of the HOMOs of the constituent closed shell EDO-TTF molecules (see Fig. 3). The HOMO−3 is the fully bonding combination. Each subsequent tetramer orbital is more anti-bonding and the tetramer HOMO is the fully anti-bonding combination of the molecular HOMOs.

Next, we allow charge transfer by adding two electron accepting PF_6 molecules to the EDO-TTF tetramer stack, *i.e.* the $(EDO-TTF)_4(PF_6)_2$ unit cell is created. The PF_6 molecules essentially remove two electrons from the fully anti-bonding HOMO of the EDO-TTF tetramer which, now becomes the LUMO of the unit cell. The PF_6 molecular orbitals are lower in energy and hardly mix with the frontier orbitals of the EDO-TTF stack. In the crystal, it is expected that the lowest conduction band and highest three valence bands are similar in nature to the MOs shown here. For a further detailed discussion of the electronic structure of the unit cell cluster we refer to our recent paper.[18]
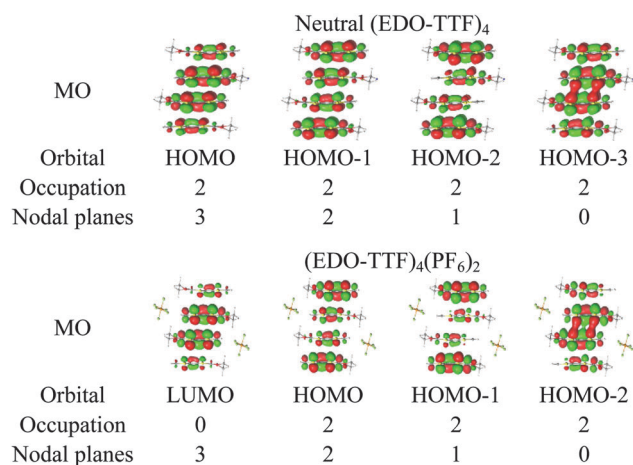

Fig. 3 Frontier orbitals of neutral $(EDO-TTF)_4$ (left) and $(EDO-TTF)_4(PF_6)_2$ (right), their occupation and the number of nodal planes between molecular MOs.

Band structures and densities of states

For the crystals, band structures and density of states (DOS) were computed. Three different scans through the Brillouin zone (BZ) were made for the LT and HT crystals. The main purpose of the first scan is to make the connection of the bands to the cluster HF MOs. We examine the band dispersion in the main directions in the crystal structures (see Fig. 4). These band dispersion plots are expected to be different because the cell parameters are different for the two crystals. A second scan was performed to study the band dispersion in the main directions of translational symmetry (see Fig. 5). The orientation of the molecules is not identical in the two crystals. To enable a better analysis of the intermolecular interactions a third scan was performed in the main molecular directions (see Fig. 6 and 7).

The band structure and DOS calculated for the experimental X-ray crystal structures is shown in Fig. 4. Our B3LYP band structures are nearly identical to the PBE0 results, which shows that our results are not affected by our choice of using 20% or 25% of Fock exchange in the functional. We choose to only present the HF and PBE0 results. In the band structures, the lowest conduction band is labelled φ_1, the highest valence bands φ_2–φ_4. From atom projected DOS it is concluded, as predicted from our cluster calculations, that these four bands have EDO-TTF character and have negligible contributions from PF_6. The conducting nature of the crystals is confirmed. The LT crystal exhibits a valence-conduction band gap. Also the (0110) CO was reproduced. The CO in the HT crystal is confirmed to be $(\frac{1}{2}\frac{1}{2}\frac{1}{2}\frac{1}{2})$
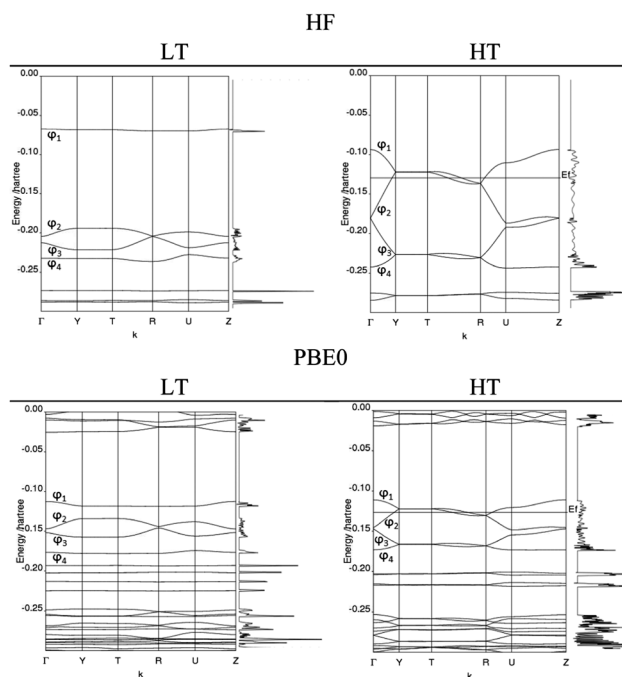
Fig. 4 Band structure and DOS obtained with HF and PBE0 for the LT and HT crystals. Symbols Γ, Y, T, R, U, Z refer to k-points in the BZ of which the coordinates are expressed in fractional coordinates $a*$,$b*$,$c*$ as follows: Γ = (0,0,0), Y = (0,$\frac{1}{2}$,0), T = (0,$\frac{1}{2}$,$\frac{1}{2}$), R = ($\frac{1}{2}$,$\frac{1}{2}$,$\frac{1}{2}$), U = ($\frac{1}{2}$,0,$\frac{1}{2}$), Z = (0,0,$\frac{1}{2}$). Zero energy is taken from the orbital energies of the respective methods.

Fig. 5 PBE0 band structure and DOS for the LT (a) and HT (d) crystal built from unit cells defined by the three main translational directions. Unit cell top view (b and e) and side view (c and f). The symbols $\varphi_1-\varphi_4$ refer to the four frontier crystal orbitals. The symbols Γ, X, V, Z, U, R refer to the points in the BZ of which the coordinates are expressed in fractional coordinates a^*,b^*,c^* as follows: $\Gamma = (0,0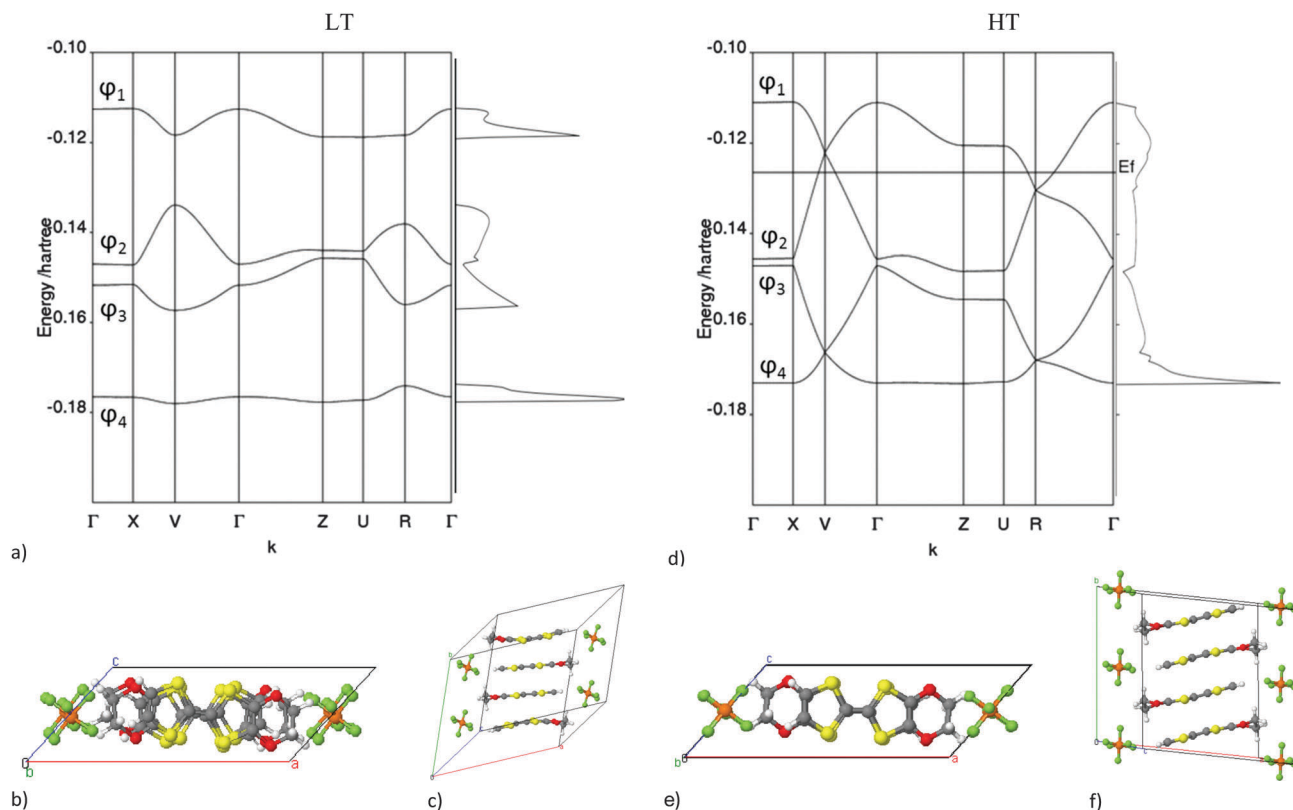,0)$, $X = (\frac{1}{2},0,0)$, $V = (\frac{1}{2},\frac{1}{2},0)$, $Z = (0,0,\frac{1}{2})$, $U = (\frac{1}{2},0,\frac{1}{2})$, $R = (\frac{1}{2},\frac{1}{2},\frac{1}{2})$.
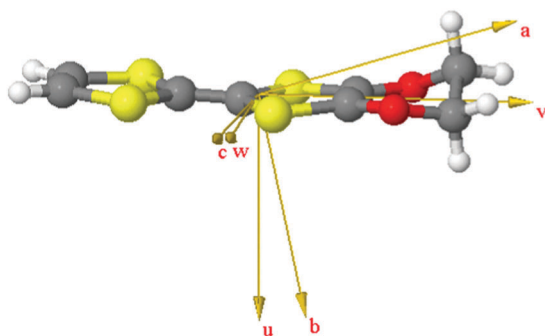

Fig. 6 Translational directions {**a**,**b**,**c**} and the principal axis of inertia {**u**,**v**,**w**} of a planar EDO-TTF molecule in the HT crystal.

and with a partially filled valence band it is a band conductor. Using RHF we also found for the HT crystal an insulating state 5 kcal mol^{-1} lower in energy with a (0110) CO. This result highlights the CO instability. The well-known overestimation of the HF band gap is apparent in the band structure of the insulating LT crystal. The bands are relatively flat. The smaller band widths in the LT crystal indicate smaller interactions between unit cells than in the HT crystal. There is qualitative agreement between the band structures obtained with HF and PBE0. The HF bands show more dispersion. PBE0 is our functional of choice for the remainder of this article. The band

gap compares well to experiment (*vide infra*). For a better comparison of the band dispersion we use, in the next sections, transformed unit cells for our analysis in which the cell parameters are comparable.

Dispersion along the main translational directions

The distinctions in the band dispersion of the four frontier crystal orbitals were analysed by scanning along the main three directions of translational symmetry (see Fig. 5). To enable this analysis, the original lattice was transformed (see ESI†) to contain one EDO-TTF tetramer stack (Fig. 5c and f). The resulting band structures are shown in Fig. 5a and d. Please note that φ_1 (φ_2) is partially occupied (unoccupied) in the HT phase. The Bloch orbitals of φ_1 and φ_2 are similar to the MOs in the unit cell clusters (see Fig. 3). At the gamma point the amplitudes on each monomer are equal. However at the edge of the BZ in the **b*** direction, φ_1 is more localised on the inner EDO-TTF molecules and φ_2 more on the outer molecules. This is the case in both the LT and HT crystals. This leads to the view that dimers in the HT phase are more anti-bonding compared to dimers in the LT phase. In going from HT to LT, the bands φ_1 and φ_2 become separated, a band gap forms, and the dimers become more bonded.
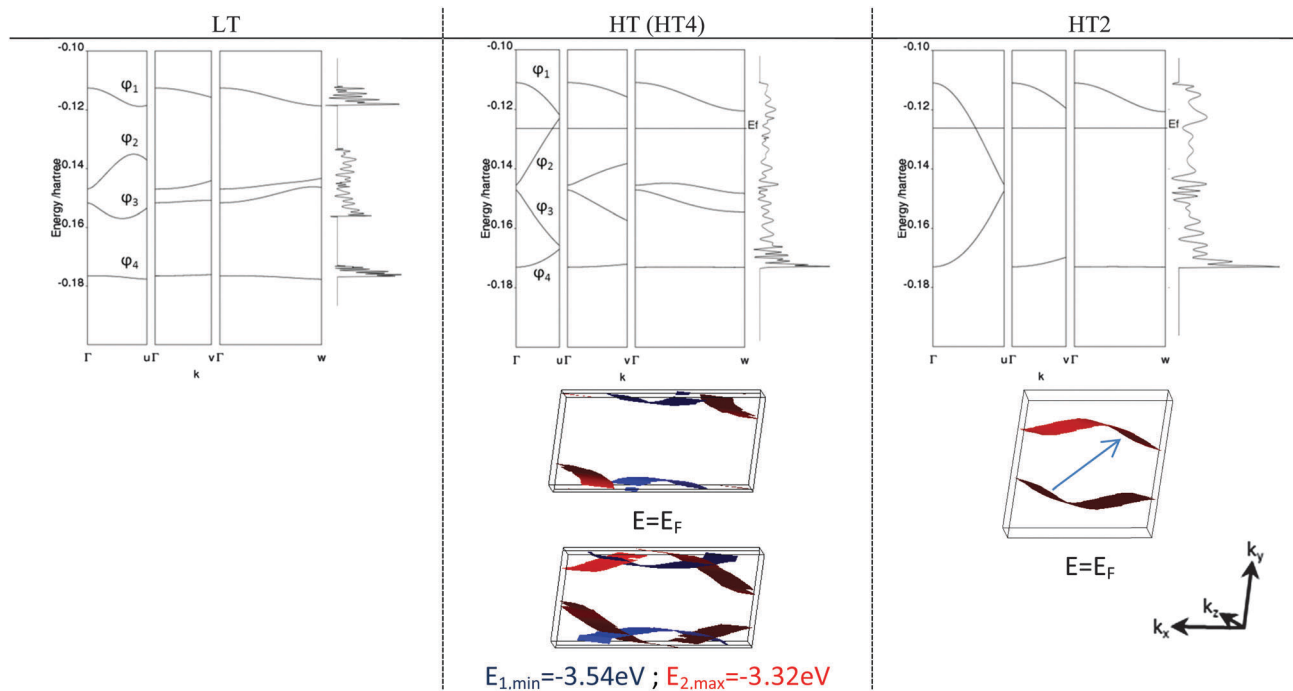
Fig. 7 PBE0 band structure from Γ to the directions $\{u,v,w\}$ and the DOS diagrams in the LT, HT4 and the HT2 crystal. Fermi surface in the HT4 and HT2 crystals (see text). The arrow indicates the nesting vector.

Dispersion in molecular directions

The orientation of the EDO-TTF molecules with respect to the **b** axis is different in the two crystals. For a better study of the inter-molecular interactions a third band dispersion diagram was made based on the interesting molecular directions, *i.e.* along the three principal axes of inertia of the (planar) EDO-TTF molecules (see Fig. 6 and the ESI† for details).

Fig. 7 clearly shows that most interaction and therefore most band dispersion occurs in the EDO-TTF stacking direction **u**. The extremes in the band structure toward the BZ boundary is an indication that vectors **u** and **b*** are not precisely in the same direction. Intermolecular interactions can be quantified by means of the hopping integral t from the tight binding model for a one-dimensional chain. In this model the width of the band dispersion Δ is related to t as $\Delta = 4|t|$. Because $\Delta u > \Delta v > \Delta w$ for the bands shown, it follows that $|t_u| > |t_v| > |t_w|$ (see Table S2 in the ESI†). Therefore the conductivity is expected to be predominant in the **u** direction. The Q1D conduction nature is also visible from the HT band dispersion diagram in the Fig. 7. The highest two valence bands, φ_1 and φ_2 are partially overlapping approximately at the Fermi energy. These bands span the energy domain $[-3.02, -4.04\ \text{eV}]$, the domain of overlap is $[-3.55, -3.33\ \text{eV}]$ and $E_F = -3.44\ \text{eV}$. The intersection, however, is only visible in the stacking direction **u**. In the other two directions these bands are not intersecting with the Fermi level. Therefore, strictly reasoning within band theory, the crystal is an insulator in these directions.

In the insulating LT crystal, in Fig. 7 it is observed that a band gap is formed: a Peierls gap. The dispersion of the LT

bands φ_1 and φ_2 in the **u** direction is smaller than that in the HT crystal. Where these bands overlap in the HT crystal, in the LT crystal they are separated by 0.40 eV. From the band structure obtained with the HT2 unit cell we see clearly that one needs to consider a unit cell doubling for a band gap to form. The Fermi level in the HT2 crystal intersects roughly midway through the highest valence band. The bands fold when doubling the number of molecules creating the HT4 (HT) unit cell. The Fermi level is at the intersection of these bands. The deformations present in the LT lattice, the slight dimerisation of dimers and perhaps also the geometrical deformation of half of the near planar EDO-TTF molecules to a bent geometry are the cause for the Peierls gap to form.

Analysis of Fermi surfaces shows also that it is necessary to consider the HT4 crystal to study the phase change. First we note that the shape of the Fermi surface (see HT2 surface in Fig. 7) confirms the Q1D nature of the conduction. It consists of two separated sheets that are slightly warped. A Fermi surface consisting of separated sheets is an indication of one dimensionality and the slight warping indicates small 2D conductivity. The nesting vector $\mathbf{n} = 2\mathbf{k}_F$, indicated by the arrow, connects the two sheets: $\varepsilon(\mathbf{k}) = \varepsilon(\mathbf{k} - \mathbf{n})$. In this crystal, the Fermi surface has contributions from φ_1 and φ_2. The Fermi surface is located right at the edge of the BZ. To indicate the overlapping bands extend further into the BZ, the energy surfaces are also plotted at the extremes of the overlapping domain. This region in k-space where the two bands overlap is rather large. Because crystal orbital φ_2 is more bonding than φ_1, the band overlap may provide the conditions for a lowering in total energy when the lattice distorts toward a more bonding dimer at LT. The surface of

φ_1 may be pushed out of the first BZ, φ_2 may be lowered in energy and become fully occupied. Or, reasoned the other way around, the deformation of the lattice may be due to interactions of the electrons. In the region of overlap, the bands mix to form a bonding and anti-bonding combination. The energy gap between them reflects the strength of the interaction. In summary, the phase transition can best be analysed using the HT4 unit cell containing four molecules.

Although this is no direct proof for the Peierls effect, it is reasonable to conclude from these results that these deformations of the lattice can stabilise the electrons in the stacking direction with the consequence that the valence band is lowered in energy. The Peierls gap has formed.

Band gap and the Fermi level

Different computational methods lead to different band gaps E_g of the LT crystal and Fermi energies E_F of the HT crystal. The HF band gap of the LT crystal is 3.38 eV and the hybrid DFT band gap is 0.40 eV (0.30 eV) using the PBE0 (B3LYP) functional. Experimentally the band gap was determined at 0.35 eV.[4] It is generally known that HF overestimates the band gap and that the band gap obtained with traditional DFT underestimates it. The success of hybrid-DFT functionals is sometimes attributed to the mixing in of the HF exchange which drives the conduction band to higher energies. Our hybrid DFT band gaps compare well with the experiment. The Fermi energy E_F was calculated at -3.52, -3.16 and -3.44 eV using HF, B3LYP and PBE0 methods respectively.

Conclusions and discussion

The band structure and density of states of the low and high temperature phases of $(EDO\text{-}TTF)_2PF_6$ using periodic HF and hybrid density functional calculations have been discussed. Our results confirm the insulating (at LT) and conducting (at HT) nature. Their respective CO is confirmed to be (0110) and $(\frac{1}{2}\frac{1}{2}\frac{1}{2}\frac{1}{2})$, with the side note that an insulating (0110) ordered RHF solution was also found at almost the same energy at HT. At LT, the (0110) CO corresponds to a geometrical ordering of (BPPB) and at HT the $(\frac{1}{2}\frac{1}{2}\frac{1}{2}\frac{1}{2})$ CO corresponds to (PPPP). We hypothesise both phases to be connected by out of plane molecular deformations. These could average an (PBBP/0110) and (BPPB/1001) ordering to become (PPPP/$\frac{1}{2}\frac{1}{2}\frac{1}{2}\frac{1}{2}$) similar to the ordering in the HT phase.

The electronic properties obtained with the hybrid functionals were found to be in good agreement with experiment. The recognition that the lowest conduction band is the fully anti-bonding combination of the HOMOs of the neutral EDO-TTF molecules, leads to the realisation that its partial population at HT reduces the bonding between EDO-TTF_2^+ dimers. The analysis of the crystal as interacting EDO-TTF_2^+ dimers, $(EDO\text{-}TTF_2^+)_2(PF_6^-)_2$, is useful. The frontier bands originate from EDO-TTF molecules. The view in terms of EDO-TTF_2^+ dimers arises as follows. The geometrical ordering at LT is associated with the localisation of

charge on the planar molecules, one in each dimer. The two cation dimers in the unit cell interact and their interplay forms the basis for the phase transition. Compared to the situation at HT, the stronger bonding of the cation dimers at LT lowers the valence band and it raises the conduction band. A gap separates the fully anti-bonding conduction band from the more bonding valence band. The small cost for making the geometrical deformations of half of the EDO-TTF molecules is likely to be compensated by the electronic stabilisation of the cationic dimers. In this view the transition is a Peierls transition.

The PF_6^- anions are closed shell entities. Their MOs do not mix with the frontier bands and the anions are spectator molecules in this sense. The anion disorder instability of the system may be more electrostatic in nature or stem from the anion contribution in vibrational modes. The system therefore consists of stacks of cations in which the conduction takes place and stacks of anions that separate the conduction stacks.

The dispersion of the bands shows that the strongest interactions occur in one dimension namely the EDO-TTF stacking direction. Interactions in the intra-sheet direction are smaller, and the inter-sheet interactions are even smaller. Therefore, the conduction is confirmed to be quasi one-dimensional. This is also confirmed from the shape of the Fermi surface. It consists of two separate sheets, a signature of a 1D conductor, and the warping of the sheets indicate that interactions in a second direction are not negligible.

At high temperature the band dispersion shows an overlap between the conduction and valence band. The Fermi level is positioned in the middle of this region of overlap. The Fermi surface satisfies a nesting condition: the two sheets of the Fermi surface are connected by a $2\mathbf{k}_F$ nesting vector. It connects points on the sheets where $\varepsilon(\mathbf{k}) = \varepsilon(-\mathbf{k})$. It is well known that this condition causes the conducting phase to be unstable with respect to the formation of the CO.[3] Small geometrical deformations may shift the bands to remove the region of overlap. This will destroy the Fermi surface and break the nesting condition. The CO phase forms and the system becomes an insulator.

Notes and references

1 K. Saito, S. Ikeuchi, A. Ota, H. Yamochi and G. Saito, *Chem. Phys. Lett.*, 2005, **401**, 76.

2 S. Aoyagi, K. Kato, A. Ota, H. Yamochi, G. Saito, H. Suematsu, M. Sakata and M. Takata, *Angew. Chem., Int. Ed.*, 2004, **43**, 3670–3673.

3 M. Yamochi and S. Koshihara, *Sci. Technol. Adv. Mater.*, 2009, **10**, 024305.

4 T. Murata, X. Shao, Y. Nakano, H. Yamochi, M. Uruichi, K. Yakushi, G. Saito and K. Tanaka, *Chem. Mater.*, 2010, **22**, 3121–3132.

30376 | *Phys. Chem. Chem. Phys.*, 2015, **17**, 30371–30377

This journal is © the Owner Societies 2015

5 O. Drozdova, K. Yakushi, K. Yamamoto, A. Ota, H. Yamochi, G. Saito, H. Tashiro and D. Tanner, *Phys. Rev. B: Condens. Matter Mater. Phys.*, 2004, **70**, 075107.

6 G. J. Linker, P. H. M. van Loosdrecht, P. Th. van Duijnen and R. Broer, *Chem. Phys. Lett.*, 2010, **487**, 220–225.

7 G. J. Linker, P. H. M. van Loosdrecht, P. Th. van Duijnen and R. Broer, *J. Phys. Chem. A*, 2012, **116**, 7219–7227.

8 P. Delheas, C. Coulon, J. Amiell, S. Frandrois, E. Toreilles, J. M. Fabre and L. Giral, *Mol. Cryst. Liq. Cryst.*, 1979, **50**, 43–58.

9 K. Bechgaard, C. S. Jacobsen, K. Mortensen, H. J. Pedresen and N. Thorup, *Solid State Commun.*, 1980, **33**, 1119.

10 C. Coulon, P. Delheas, S. Flandrois, R. Lagnier, E. Bonjour and J. M. Fabre, *J. Phys.*, 1982, **43**, 1059–1067.

11 D. Jérome, A. Mazaud, M. Ribault and K. Bechgaard, *J. Phys. Lett.*, 1980, **41**, L95.

12 *The Physics of Organic Superconductors and Conductors*, ed. A. Lebed, Springer Series in Materials Science, 2008, vol. 110.

13 J. Moser, M. Gabay, P. Auban-Senzier, D. Jérome, K. Bechgaard and J. M. Fabre, *Eur. Phys. J. B*, 1998, **1**, 39–46.

14 A. Ota, H. Yamochi and G. Saito, *J. Mater. Chem.*, 2002, **12**, 2600.

15 K. Yonemitsu, *Crystals*, 2012, **2**, 56–77.

16 M. Sakata, M. Maesato, A. Ota, H. Yamochi and G. Saito, *Synth. Met.*, 2005, **153**, 393.

17 M. Chollet, L. Guerin, N. Uchida, S. Fukaya, H. Shimoda, T. Ishikawa, H. Yamochi, G. Saito, R. Tazaki and S. Adachi, *et al.*, *Science*, 2005, **307**, 86.

18 G. J. Linker, P. Th. van Duijnen, P. H. M. van Loosdrecht and R. Broer, *Comput. Theor. Chem.*, 2015, **1069**, 105.

19 C. Adamo and V. Barone, *J. Chem. Phys.*, 1999, **110**, 6158.

20 R. Dovesi, R. Orlando, B. Civalleri, C. Roetti, V. R. Saunders and C. M. Zicovich-Wilson, *Z. Kristallogr.*, 2005, **220**, 571.

21 R. Dovesi, V. R. Saunders, C. Roetti, R. Orlando, C. M. Zicovich-Wilson, F. Pascale, B. Civalleri, K. Doll, N. M. Harrison, I. J. Bush, P. D'Arco and M. Llunell, *CRYSTAL 2009 User's Manual*, University of Torino, Torino, 2009.

22 B. Searle, *Comput. Phys. Commun.*, 2001, **137**, 25–32.

23 G. Karlström, R. Lindh, P.-Å. Malmqvist, B. O. Roos, U. Ryde, V. Veryazov, P.-O. Widmark, M. Cossi, B. Schimmelpfennig, P. Neogrady and L. Seijo, *Comput. Mater. Sci.*, 2003, **28**, 222.

This journal is © the Owner Societies 2015

Phys. Chem. Chem. Phys., 2015, **17**, 30371–30377 | **30377**